Available online at www.sciencedirect.com
SCIENCE DIRECT®
ELSEVIER
International Journal of Solids and Structures 43 (2006) 2091–2109
INTERNATIONAL JOURNAL OF SOLIDS and STRUCTURES
www.elsevier.com/locate/ijsolstr

Coplanar propagation paths of 3D cracks in infinite bodies loaded in shear

Elie Favier, Véronique Lazarus *, Jean-Baptiste Leblond

Laboratoire de Modélisation en Mécanique, Université Pierre et Marie Curie (Paris VI), Tour 65-55, Case 162, 4 place Jussieu, 75252 Paris Cedex 05, France

Received 15 December 2004; received in revised form 15 June 2005
Available online 18 August 2005

Abstract

Bower and Ortiz, recently followed by Lazarus, developed a powerful method, based on a theoretical work of Rice, for numerical simulation of planar propagation paths of mode 1 cracks in infinite isotropic elastic bodies. The efficiency of this method arose from the need for the sole 1D meshing of the crack front. This paper presents an extension of Rice's theoretical work and the associated numerical scheme to mixed-mode (2 + 3) shear loadings. Propagation is supposed to be channeled along some weak planar layer and to remain therefore coplanar, as in the case of a geological fault for instance. The capabilities of the method are illustrated by computing the propagation paths of cracks with various initial contours (circular, elliptic, rectangular, heart-shaped) in both fatigue and brittle fracture. The crack quickly reaches a stable, almost elliptic shape in all cases. An approximate but accurate analytic formula for the ratio of the axes of this stable shape is derived.

Keywords: 3D fracture mechanics; Coplanar crack propagation paths; Mode 2 + 3; Brittle fracture; Fatigue; Stable shape; Perturbation method; Weight functions

1. Introduction

There are several more or less efficient methods for numerical simulation of propagation paths of 3D cracks in elastic media. The most classical and general one is the finite element method (FEM). A

* Corresponding author. Tel.: +33 144278717; fax: +33 144275259.
E-mail addresses: favier@lmm.jussieu.fr (E. Favier), vlazarus@ccr.jussieu.fr (V. Lazarus), leblond@lmm.jussieu.fr (J.-B. Leblond).

0020-7683/$ - see front matter
doi:10.1016/j.ijsolstr.2005.06.041

non-trivial example involving a complex, non-planar crack shape is provided in the work of Xu et al. (1994). But the FEM requires meshing the whole 3D cracked body at each step of the crack propagation, and it is difficult to do this automatically. A recent and efficient variant of the FEM consists of coupling the level set method and the extended finite element method (XFEM); see for instance, Sukumar et al. (2003), Moes et al. (2002), Gravouil et al. (2002).

The sole meshing of the initial geometry is then required. Another alternative consists of using the boundary element method (BEM), which requires only 2D meshing of the crack surface and the outer boundary. Several examples of such an approach are provided in Chapter 5 of Bonnet (1994)'s book. Methods based on integral equations are especially attractive for infinite bodies since the sole meshing of the crack surface is then necessary; see for instance the examples provided by Fares (1989) and Xu and Ortiz (1993). If, in addition, the crack propagates along a plane, compelling methods requiring the sole 1D meshing of the crack front are envisageable. Using an earlier theoretical work of Rice (1989) and Bower and Ortiz (1990, 1991, 1993) proposed such an approach and applied it to various problems of practical interest. Lazarus (2003) later defined a simplified variant of this method which resulted in no significant loss of numerical accuracy.

More specifically, the basis of Bower and Ortiz' method and Lazarus' variant was Bueckner–Rice's weight function theory. The 2D version of this theory was expounded by Bueckner (1970) and Rice (1972), and its extension to the 3D case by Rice (1972) (in the appendix of this reference) and Bueckner (1973). It was applied by Rice (1989) to planar cracks with arbitrary contours loaded in mode 1. The theory yielded, to first order, the variation of the mode 1 stress intensity factor (SIF) along the crack front arising from some small but otherwise arbitrary coplanar perturbation of this front, under conditions of constant prescribed loading. This variation was expressed as a line integral over the unperturbed front which involved, in addition to the perturbation, some geometry-dependent "kernel" linked to the mode 1 weight function. The theory also provided the variation of this kernel, again to first order, in a similar form. Bower and Ortiz (1990, 1991, 1993)'s method consisted of applying Rice's two formulae to some sequence of small perturbations of the front resulting in arbitrary deformation of its initial shape. They applied it to the study of the propagation paths of semi-infinite tensile cracks in heterogeneous media, in both fatigue and brittle fracture.

In Lazarus (2003)'s variant, the numerical procedure was greatly simplified by using linear instead of quadratic elements, calculating the crack advance and the various integrals at the same discretization points instead of distinguishing between nodes and collocation points, etc. Validation tests based on numerical calculation of SIFs for crack geometries for which some analytical solution existed showed that such simplifications did not affect the overall numerical accuracy. In fact, the only point that was found to really require special care was accurate evaluation of some integrals in principal value. Also, Lazarus replaced the Irwin–Griffith propagation law for brittle fracture used by Bower and Ortiz by that of Paris. Nothing was lost by doing so since as noted by Lazarus, in addition to being a good propagation law for fatigue, Paris' law "simulates" Irwin–Griffith's law in the limit of very large Paris exponent. The advantage of using Paris' law was that the crack advance at all time steps and discretization points was directly provided by some explicit formula. In contrast, deducing the crack advance at the discretization points from the Irwin–Griffith criterion, as was done by Bower and Ortiz, was more difficult in two respects. First, iterations were required to determine the "active" part of the front, that is that portion which effectively propagates at the instant considered. Second, for each iteration, it was necessary to solve a large system of linear equations on the unknown values of the crack front advance at the discretization points of this active part. Lazarus applied her method to the study of the propagation paths, in fatigue and brittle fracture, of initially elliptic, rectangular and heart-shaped cracks loaded through some uniform remote tensile stress. She found that for all of these initial configurations, the crack quickly reached a stable, circular shape.

Bower and Ortiz' method and Lazarus' variant were developed only for mode 1 cracks. The aim of this paper is to extend Lazarus' method to mixed-mode (2 + 3) loadings, and to illustrate it through several examples of simulation of propagation of shear mode cracks with simple initial shapes, in both fatigue and brittle fracture. Propagation will be assumed to be coplanar; this is reasonable provided that the crack is channeled along a weak planar layer, which is the case, for instance, for a geological fault.

The first step consists of extending Rice (1989)'s results to planar cracks with arbitrary contour loaded in mode 2 + 3. This is done in Section 2. Our starting point here is Rice (1985)'s general formula (applicable to all modes) for the first-order variation of the displacement discontinuity across the crack plane resulting from some small coplanar advance of the front, under conditions of constant prescribed loading. The first-order variation of the SIFs is deduced from there by letting the observation point of this discontinuity tend toward the crack front. The treatment here extends both that of Rice (1989), which applied to planar mode 1 cracks with arbitrary contour, and those of Gao and Rice (1986) and Gao (1988), which applied to planar shear mode cracks with straight or circular contour. The first-order variation of the relevant kernels is also derived in a similar way, using their relation to the weight functions. Section 3 then briefly presents the extension of Lazarus (2003)'s numerical method to shear loadings. This extension is straightforward in principle, but the extended method is notably heavier than the original one for mode 1, because of the inevitable coupling of modes 2 and 3. Section 4 expounds validation tests based on numerical calculation of the distribution of SIFs along the front of elliptic cracks loaded in shear. Finally, Section 5 presents applications in the form of computation of planar propagation paths of shear mode cracks with simple (circular, elliptic, rectangular and heart-shaped) initial contours, in fatigue and brittle fracture. It is found that the crack front quickly reaches some stable, almost elliptic shape in all cases. An approximate but accurate analytic formula for the ratio of the axes of this stable shape is derived.

2. Extension of Rice's formulae to modes 2 and 3

2.1. Definitions and notations—Elementary properties of weight functions

2.1.1. Stress intensity factors

Consider a plane crack of arbitrary shape embedded in some infinite isotropic elastic medium subjected to some arbitrary loading (Fig. 1). Let $\mathscr{F}$ denote the crack front and s some curvilinear abscissa along it. At each point s of $\mathscr{F}$, define a local basis of vectors $(\vec{e}_1(s), \vec{e}_2(s), \vec{e}_3(s))$ in the following way:

(1) $\vec{e}_3(s)$ is tangent to $\mathscr{F}$ and oriented in the same direction as the curvilinear abscissa s;
(2) $\vec{e}_2(s)$ is in the crack plane, orthogonal to $\mathscr{F}$ and oriented in the direction of propagation;

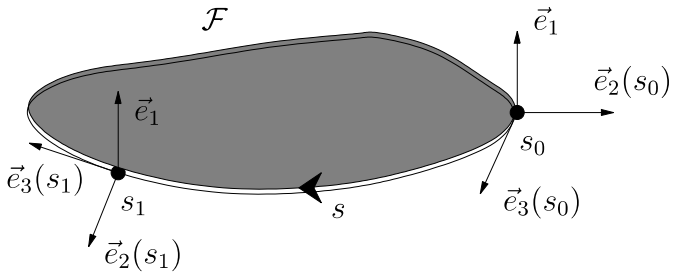

Fig. 1. Notations for a planar crack with arbitrary contour.

(3) $\vec{e}_1(s) \equiv \vec{e}_1$ is orthogonal to the crack plane and oriented in such a way that the basis $(\vec{e}_2(s), \vec{e}_1, \vec{e}_3(s))$ is direct.[1]

The SIFs $K_j(s)$, $j = 1,2,3$ at point s are then defined by the following formula, where Einstein's summation convention is employed:

$$\lim_{r\to 0} \sqrt{\frac{2\pi}{r}} [\![\vec{u}(s,r)]\!] \equiv 8\Lambda_{ij} K_j(s) \vec{e}_i(s) \tag{1}$$

In this expression $[\![\vec{u}(s,r)]\!]$ denotes the displacement discontinuity across the crack plane, oriented by the vector $\vec{e}_1$, at the distance r behind the point s of $\mathscr{F}$, in the direction of the vector $-\vec{e}_2(s)$. Also, $(\Lambda_{ij})_{1\leqslant i\leqslant 3, 1\leqslant j\leqslant 3} \equiv \mathbf{\Lambda}$ is the diagonal matrix defined by

$$\mathbf{\Lambda} \equiv \frac{1}{E} \begin{pmatrix} 1-\nu^2 & 0 & 0 \\ 0 & 1-\nu^2 & 0 \\ 0 & 0 & 1+\nu \end{pmatrix} \tag{2}$$

where E denotes Young's modulus and ν, Poisson's ratio.[2]

2.1.2. Crack face weight functions and fundamental kernels

Let $k_{ij}(\mathscr{F}; s'; s, r)$ denote the ith SIF at the point s' of the crack front $\mathscr{F}$ resulting from application of a pair of opposite unit point forces equal to $\pm\vec{e}_j(s)$ on the upper (+) and lower (−) crack surfaces at a distance r behind the point s of the crack front. These nine scalar functions are called the *crack face weight functions* (CFWFs).

The functions $k_{ij}(\mathscr{F}; s'; s, r)/\sqrt{r}$ are known to have a well-defined limit for $r \to 0$ (see for instance, Leblond et al. (1999)). We then define the matrix $(W_{ij}(s', s))_{1\leqslant i\leqslant 3, 1\leqslant j\leqslant 3} \equiv \mathbf{W}(s', s)$ by the formula

$$W_{ij}(s', s) \equiv \pi \sqrt{\frac{\pi}{2}} D^2(s, s') \lim_{r\to 0} \frac{k_{ij}(\mathscr{F}; s'; s, r)}{\sqrt{r}} \tag{3}$$

where $D(s, s')$ denotes the cartesian distance between points s and s'. The functions $W_{ij}(s', s)$ in fact depend on the crack front shape, just like the CFWFs, but the argument $\mathscr{F}$ is omitted here for conciseness. They will be called the *fundamental kernels* or more shortly the *kernels*.

The CFWFs are positively homogeneous of degree $-3/2$; that is, if all distances are multiplied by some positive factor λ, the CFWFs are multiplied by $\lambda^{-3/2}$. The definition (3) of the functions $W_{ij}(s', s)$ then implies that they are positively homogeneous of degree 0.

Since tensile and shear problems are uncoupled for a planar crack in an infinite body, whatever the shape of the crack front, the components k_{12}, k_{13}, k_{21} and k_{31} of the CFWFs are zero, so that by Eq. (3):

$$W_{12}(s', s) \equiv W_{13}(s', s) \equiv W_{21}(s', s) \equiv W_{31}(s', s) \equiv 0. \tag{4}$$

Finally, considering two problems, one with point forces equal to $\pm\vec{e}_i$ exerted on the crack faces at (s, r) and one with point forces equal to $\pm\vec{e}_j$ exerted on the crack faces at (s', r'), applying Betti's theorem, and using Eqs. (1) and (3), one sees that the kernels obey the following "symmetry" property:

$$\Lambda_{im} W_{mj}(s, s') = \Lambda_{jm} W_{mi}(s', s) \tag{5}$$

[1] This choice differs from the usual one but coincides with that made by Rice (1989). Its advantage is that the basis vectors are labelled to agree with mode number designations for the SIFs, and this simplifies the reasoning below leading to the expressions of the variations of these SIFs when the crack front is perturbed.

[2] A similar formula holds for an arbitrary anisotropic medium but the matrix $\mathbf{\Lambda}$ is then no longer diagonal.

2.2. Principle of the derivation of the variations of the stress intensity factors and fundamental kernels

Let us now assume that the crack advances, under constant loading, by a small distance $\delta a(s)$ within its plane in the direction perpendicular to its front. The variation of the displacement discontinuity $\delta[\![\vec{u}(s_0,r)]\!]$ at point (s_0,r) is given, to first order in the perturbation, by the following formula Rice (1985):

$$\delta[\![\vec{u}(s_0,r)]\!] = 2\Lambda_{jm}\vec{e}_i(s_0)\int_{\mathscr{F}} k_{ji}(\mathscr{F};s;s_0,r)K_m(s)\delta a(s)\,\mathrm{d}s. \tag{6}$$

The variations of the SIFs will be obtained from there by taking the limit $r \to 0$ in this expression, using their relation to the variation of the displacement discontinuity. In fact, the formula for $\delta K_1(s_0)$ was given by Rice (1989) for a planar crack with arbitrary contour, and those for $\delta K_2(s_0)$ and $\delta K_3(s_0)$, which are of more interest here, by Leblond et al. (1999) for arbitrary, not necessarily planar initial crack geometries, and arbitrary, even possibly kinked, small crack extensions. (Leblond et al. (1999)'s formula in fact extended previous formulae of Gao and Rice (1986) and Gao (1988) which applied to planar shear mode cracks with coplanar extension and straight or circular contour.) However we shall re-derive Leblond et al. (1999)'s formulae here, for two reasons.

(1) The hypothesis of coplanar crack extension makes it possible to greatly simplify Leblond et al. (1999)'s intricate reasoning. Presenting the simple[3] reasoning proposed below offers the advantage that the paper is self-contained at little additional cost.
(2) It will also be necessary to calculate the variations of the kernels since these kernels appear in the formulae for the variations of the SIFs. The derivation of these additional formulae will use a similar, albeit somewhat more complex reasoning, based on the fact that the kernels are related to the CFWFs and thus to some SIFs generated by special loadings. The presentation of the derivation of the formulae for the variations of the SIFs will serve as a useful introduction there.

The formulae for $\delta W_{22}(s_0,s_1)$, $\delta W_{33}(s_0,s_1)$, $\delta W_{23}(s_0,s_1)$ and $\delta W_{32}(s_0,s_1)$ provided below are new. In contrast, it has already been mentioned in Section 1 that the formula for $\delta W_{11}(s_0,s_1)$ was provided by Rice (1989). We shall however re-derive it at no additional cost, since the reasoning presented below applies indifferently to all modes.

2.3. Variation of the stress intensity factors

In a first step, we assume that δa is zero at that point s_0 where the δK_i are to be evaluated (Fig. 2). The basis $(\vec{e}_1^*(s_0)\equiv\vec{e}_1,\vec{e}_2^*(s_0),\vec{e}_3^*(s_0))$ "adapted" to the perturbed crack front at this point is obtained, to first order in the perturbation, through rotation of the old one $(\vec{e}_1(s_0)\equiv\vec{e}_1,\vec{e}_2(s_0),\vec{e}_3(s_0))$ by an angle $\mathrm{d}\delta a(s_0)/\mathrm{d}s \equiv \delta a'(s_0)$ about the vector $\vec{e}_1$. Hence

$$\vec{e}_i^*(s_0) = \vec{e}_i(s_0) + \delta a'(s_0)\vec{e}_1\times\vec{e}_i(s_0) \tag{7}$$

where the symbol $\times$ denotes the vector product. (Note that since the basis $(\vec{e}_1,\vec{e}_2(s_0),\vec{e}_3(s_0))$ is left-handed, $\vec{e}_1\times\vec{e}_2(s_0) = -\vec{e}_3(s_0)$ and $\vec{e}_1\times\vec{e}_3(s_0) = \vec{e}_2(s_0)$).

Let $[\![\vec{u}^*(s_0,r^*)]\!]$ denote the displacement discontinuity across the crack plane in the perturbed crack configuration, at a small distance r^* behind the point s_0 in the direction of the vector $-\vec{e}_2^*(s_0)$ (Fig. 2). By Eq. (1),

$$\lim_{r^*\to 0}\sqrt{\frac{2\pi}{r^*}}[\![\vec{u}^*(s_0,r^*)]\!] = 8\Lambda_{ij}[K_j(s_0)+\delta K_j(s_0)]\vec{e}_i^*(s_0) \tag{8}$$

[3] In principle, less so in details.

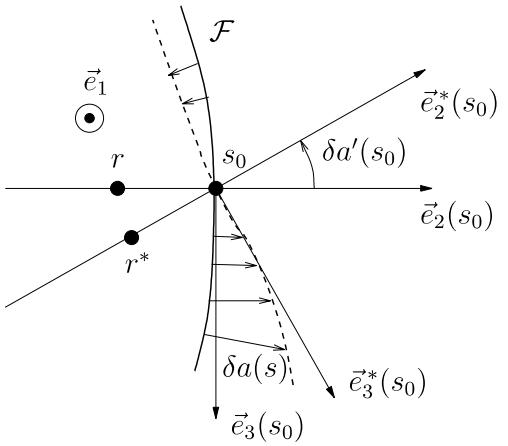

Fig. 2. Motion of the crack front around the immobile point s_0.

Now, by definition,

$$\delta[\![\vec{u}(s_0,r)]\!] \equiv [\![\vec{u}^*(s_0,r)]\!] - [\![\vec{u}(s_0,r)]\!] \tag{9}$$

where $[\![\vec{u}^*(s_0,r)]\!]$ is the displacement discontinuity in the perturbed crack configuration at a distance r behind the point s_0 in the direction of the vector $-\vec{e}_2(s_0)$, *not* $-\vec{e}_2^*(s_0)$ (Fig. 2). However the vector $-\vec{e}_2(s_0)$ here may be replaced by $-\vec{e}_2^*(s_0)$ because the resulting displacement of the observation point is of second order in the perturbation, as is obvious from Fig. 2. Using Eqs. (7) and (8), one then gets

$$\lim_{r\to 0}\sqrt{\frac{2\pi}{r}}\delta[\![\vec{u}(s_0,r)]\!] = 8\left[\Lambda_{ij}\delta K_j(s_0) + \varepsilon_{1ij}\Lambda_{jm}K_m(s_0)\delta a'(s_0)\right]\vec{e}_i(s_0) \tag{10}$$

where the ε_{ijm} denote the permutation symbols.[4]

We shall now use Eq. (6) in the limit $r \to 0$. It is shown in Appendix A that in this limit, the asymptotic behaviour of the integrals in the right-hand side is given by the following formula:

$$\begin{aligned}&\frac{\sqrt{2\pi}}{4}\lim_{r\to 0}\frac{1}{\sqrt{r}}\int_{\mathscr{F}} k_{ji}(\mathscr{F};s;s_0,r)K_m(s)\delta a(s)\,\mathrm{d}s \\ &\quad = \frac{v}{2-v}(\delta_{j2}\delta_{i3}+\delta_{j3}\delta_{i2})K_m(s_0)\delta a'(s_0) + \frac{1}{2\pi}\mathrm{PV}\int_{\mathscr{F}}\frac{W_{ji}(s,s_0)}{D^2(s_0,s)}K_m(s)\delta a(s)\,\mathrm{d}s\end{aligned} \tag{11}$$

where the δ_{ij} denote Kronecker's symbols and the integral in the right-hand side is to be understood as a Cauchy principal value (PV). Dividing then Eq. (6) by $\sqrt{r}$ and taking the limit $r \to 0$ using Eqs. (10) and (11), one obtains after some algebraic manipulations the following formula:

$$\delta\mathbf{K}(s_0) = \mathbf{N}\cdot\mathbf{K}(s_0)\delta a'(s_0) + \frac{1}{2\pi}\mathrm{PV}\int_{\mathscr{F}}\frac{\mathbf{W}(s_0,s)}{D^2(s_0,s)}\cdot\mathbf{K}(s)\delta a(s)\,\mathrm{d}s \tag{12}$$

The quantities $\mathbf{K}(s) \equiv (K_i(s))_{1\leqslant i\leqslant 3}$ and $\delta K(s) \equiv (\delta\mathbf{K}_i(s))_{1\leqslant i\leqslant 3}$ here are the column vectors of initial SIFs and variations of these SIFs, and $\mathbf{N} \equiv (N_{ij})_{1\leqslant i\leqslant 3,1\leqslant j\leqslant 3}$ is the matrix defined by

[4] $\varepsilon_{ijm} = 0$ if two indices are equal, 1 if $\{i,j,m\}$ is a positive permutation of $\{1,2,3\}$, -1 if it is a negative permutation.

$$\mathbf{N} \equiv \frac{2}{2-\nu}\begin{pmatrix} 0 & 0 & 0 \\ 0 & 0 & -1 \\ 0 & 1-\nu & 0 \end{pmatrix} \tag{13}$$

Eq. (12) is identical to Leblond et al. (1999)'s general equation (30)' (with the notation $\frac{1}{2\pi}\frac{\mathbf{W}(s_0,s)}{D^2(s,s_0)}$ instead of $\mathbf{Z}(s_0,s)$), in the special case of a planar crack with coplanar extension (and zero crack advance at the point s_0).

The restriction $\delta a(s_0)=0$ will now be removed by using a trick of Rice (1989). This trick consists of decomposing an arbitrary motion of the crack front defined by the normal advance $\delta a(s)$ into two steps:

(1) A translatory motion of displacement vector $\delta a(s_0)\vec{e}_2(s_0)$. This motion brings the point s_0 to its correct final position while leaving the crack front shape unchanged. The corresponding normal advance $\delta_* a(s)$ is given, to first order in $\delta a(s)$, by
$$\delta_* a(s) = \delta a(s_0)\vec{e}_2(s_0)\cdot\vec{e}_2(s) \tag{14}$$
The associated variation of $\mathbf{K}(s)$ will be denoted $\boldsymbol{\delta}_*\mathbf{K}(s)$.
(2) A motion with normal advance given by $\delta a(s)-\delta_* a(s)$. This advance is zero at point s_0 so that the corresponding variation of $\mathbf{K}(s_0)$ is given by Eq. (12), with $\delta a'(s_0)-\delta_* a'(s_0)=\delta a'(s_0)$ since $\delta_* a'(s_0)=0$ by Eq. (14).

Adding up the contributions from these two motions, one gets the final expression of the variation of the SIFs under constant loading in the general case:

$$\delta\mathbf{K}(s_0) = \delta_*\mathbf{K}(s_0) + \mathbf{N}\cdot\mathbf{K}(\mathbf{s_0})\delta a'(s_0) + \frac{1}{2\pi}\mathrm{PV}\int_{\mathscr{F}}\frac{\mathbf{W}(s_0,s)}{D^2(s_0,s)}\cdot\mathbf{K}(s)[\delta a(s)-\delta_* a(s)]\,\mathrm{d}s \tag{15}$$

2.4. Variation of the fundamental kernels

The method of derivation of the first-order formula for $\delta\mathbf{W}(s_0,s_1)$ consists of applying Eq. (12) to those special loadings defining the kernels, that is, pairs of opposite, unit point forces exerted on the crack faces close to the crack front.

We first make the assumption that the crack advance δa is zero at points s_0 and s_1. We also define the following CFWFs pertaining to the perturbed crack configuration:

(1) $k^*_{ij}(\mathscr{F}^*;s_0;s_1,r^*)$ is the ith SIF at point s_0 on the perturbed crack front $\mathscr{F}^*$ when point forces equal to $\pm\vec{e}^*_j(s_1)$ are applied at a distance r^* behind point s_1 on this front in the direction of the vector $-\vec{e}^*_2(s_1)$;
(2) $k^*_{ij}(\mathscr{F}^*;s_0;s_1,r)$ is defined in the same way except that the forces are exerted at a distance r behind point s_1 in the direction of the vector $-\vec{e}_2(s_1)$ instead of $-\vec{e}^*_2(s_1)$;
(3) $k_{ij}(\mathscr{F}^*;s_0;s_1,r)$ is defined in the same way as $k^*_{ij}(\mathscr{F}^*;s_0;s_1,r)$ except that the forces are equal to $\pm\vec{e}_j(s_1)$ instead of $\pm\vec{e}^*_j(s_1)$.

Suppose that forces equal to $\pm\vec{e}_j(s_1)$ are applied at a distance r behind point s_1 in the direction of the vector $-\vec{e}_2(s_1)$, and compare the ith resulting SIFs at point s_0 in the initial and perturbed configurations of the crack. Eq. (12) yields, in this specific case:

$$\begin{aligned} &k_{ij}(\mathscr{F}^*;s_0;s_1,r) - k_{ij}(\mathscr{F};s_0;s_1,r) \\ &\quad = N_{im}k_{mj}(\mathscr{F};s_0;s_1,r)\delta a'(s_0) + \frac{1}{2\pi}\mathrm{PV}\int_{\mathscr{F}}\frac{W_{im}(s_0,s)}{D^2(s_0,s)}k_{mj}(\mathscr{F};s;s_1,r)\delta a(s)\,\mathrm{d}s \end{aligned} \tag{16}$$

Now, by definition,

$$\delta W_{ij}(s_0,s_1)=\pi\sqrt{\frac{\pi}{2}}D^2(s_0,s_1)\left(\lim_{r^*\to 0}\frac{k^*_{ij}(\mathscr{F}^*;s_0;s_1,r^*)}{\sqrt{r^*}}-\lim_{r\to 0}\frac{k_{ij}(\mathscr{F};s_0;s_1,r)}{\sqrt{r}}\right) \tag{17}$$

In the first limit here, $k^*_{ij}(\mathscr{F}^*;s_0;s_1,r^*)$ may be replaced by $k^*_{ij}(\mathscr{F}^*;s_0;s_1,r)$ since the error thus introduced on the position of the point of application of the forces is of second order in the perturbation; thus

$$\delta W_{ij}(s_0,s_1)=\pi\sqrt{\frac{\pi}{2}}D^2(s_0,s_1)\lim_{r\to 0}\frac{k^*_{ij}(\mathscr{F}^*;s_0;s_1,r)-k_{ij}(\mathscr{F};s_0;s_1,r)}{\sqrt{r}} \tag{18}$$

Using now linearity with respect to the loading and Eq. (7) to express the $k^*_{ij}(\mathscr{F}^*;s_0;s_1,r)$ in terms of the $k_{ij}(\mathscr{F}^*;s_0;s_1,r)$, one gets after some manipulations

$$\begin{aligned}\delta W_{ij}(s_0,s_1)=&\pi\sqrt{\frac{\pi}{2}}D^2(s_0,s_1)\lim_{r\to 0}\frac{k_{ij}(\mathscr{F}^*;s_0;s_1,r)-k_{ij}(\mathscr{F};s_0;s_1,r)}{\sqrt{r}}\\&+\left[\delta_{j3}W_{i2}(s_0,s_1)-\delta_{j2}W_{i3}(s_0,s_1)\right]\delta a'(s_1)\end{aligned} \tag{19}$$

Inserting Eq. (16) in this result and taking the limit $r\to 0$ in the same way as in Section 2.3, using in particular equation (11), one then obtains

$$\begin{aligned}\delta\mathbf{W}(s_0,s_1)=&\mathbf{N}\cdot\mathbf{W}(s_0,s_1)\delta a'(s_0)-\mathbf{W}(s_0,s_1)\cdot\mathbf{N}\delta a'(s_1)\\&+\frac{D^2(s_0,s_1)}{2\pi}\ \mathrm{PV}\int_{\mathscr{F}}\frac{\mathbf{W}(s_0,s)\cdot\mathbf{W}(s,s_1)}{D^2(s_0,s)D^2(s_1,s)}\delta a(s)\,\mathrm{d}s\end{aligned} \tag{20}$$

In order to finally get rid of the hypothesis $\delta a(s_0)=\delta a(s_1)=0$, we use another trick of Rice (1989). This trick consists of now decomposing an arbitrary motion of the crack front, defined by the normal advance δa(s), into a motion corresponding to some advance $\delta_{**}a(s)$ and bringing points s_0 and s_1 to their correct final positions while leaving the kernels unchanged, plus a motion corresponding to the advance $\delta a(s)-\delta_{**}a(s)$, which is zero at s_0 and s_1. More specifically, one can always find a combination of a translatory motion, a rotation and a homothetical transformation bringing two distinct points s_0, s_1 from any initial positions to any final positions. (This is obvious using a complex variable formalism and noting that such transformations are of the form $f(z)=az+b$, where a and b are arbitrary complex parameters.) Such a combination does leave the kernels unaffected because they are independent of the position of the crack in its plane, its orientation and its size. Application of Eq. (20) to the second motion then yields the final expression of the variation of the kernels under constant loading in the general case:

$$\begin{aligned}\delta\mathbf{W}(s_0,s_1)=&\mathbf{N}\cdot\mathbf{W}(s_0,s_1)[\delta a'(s_0)-\delta_{**}a'(s_0)]-\mathbf{W}(s_0,s_1)\cdot\mathbf{N}[\delta a'(s_1)-\delta_{**}a'(s_1)]\\&+\frac{D^2(s_0,s_1)}{2\pi}\mathrm{PV}\int_{\mathscr{F}}\frac{\mathbf{W}(s_0,s)\cdot\mathbf{W}(s,s_1)}{D^2(s_0,s)D^2(s_1,s)}[\delta a(s)-\delta_{**}a(s)]\,\mathrm{d}s\end{aligned} \tag{21}$$

Note that quantities $\delta_{**}a'(s_0)$ and $\delta_{**}a'(s_1)$ here are nonzero, unlike quantity $\delta_{*}a'(s_0)$ in Eq. (15). The formula for the component $\delta W_{11}(s_0,s_1)$ is identical to that derived by Rice (1989).

3. Numerical procedure

3.1. General hypotheses

Formula (15) provides the first-order variation $\delta\mathbf{K}(s_0)$ of $\mathbf{K}(s_0)$ arising from some small coplanar perturbation of the crack front under conditions of constant prescribed loading, provided that the variation

$\delta_*\mathbf{K}(s_0)$ of $\mathbf{K}(s_0)$ for a translatory motion of the crack front is known. Such is notably the case for a loading consisting of uniform stresses applied at infinity; indeed $\delta_*\mathbf{K}(s_0) \equiv 0$ then. Attention is focused on this case in the sequel, and more specifically on shear loadings, since tensile ones have already been considered by Lazarus (2003).

Crack propagation is assumed to be coplanar, which is reasonable (for the shear loadings envisaged) if it is channeled along some weak planar layer. Such is the case for geological faults and certain cracks in composite materials. Propagation is assumed to be governed by the following Paris-type law:

$$\frac{\partial a}{\partial t}(s,t) = C[\mathscr{G}(s,t)]^{\beta/2} \tag{22}$$

In this expression $\partial a(s,t)/\partial t$ denotes the normal velocity of the crack front and $\mathscr{G}(s,t)$ the local energy release rate, related to the SIFs through Irwin's formula

$$\mathscr{G}(s,t) = \Lambda_{ij} K_i(s,t) K_j(s,t) \tag{23}$$

Also, C and β are material parameters called the *Paris constant* and the *Paris exponent*, respectively. Paris' law is adequate for sub-critical crack growth and fatigue, "t" being re-interpreted as "number of cycles" and "$\mathscr{G}$" as "$\Delta\mathscr{G}$" in the latter case. Following a remark of Lazarus (2003), it may also be considered, in the case of very large Paris exponent, as a kind of "regularization" of Griffith's propagation law for brittle fracture, just as, for instance, Norton's viscoplastic flow rule may be considered as a "viscoplastic regularization" of the Prandtl–Reuss plastic flow rule in the case of very large Norton exponent.

3.2. Lazarus' numerical procedure and its adaptation to shear mode cracks

If $\mathbf{K}(s_0)$ and $\mathbf{W}(s_0,s_1)$ are known for all points s_0, s_1 of some crack front, formula (15) (with $\delta_*\mathbf{K}(s_0) \equiv 0$) and (21) provide their values on any nearby front. Iterating the process, one can calculate them numerically for any arbitrarily deformed crack front. This is the common basis of Bower and Ortiz (1990)'s method for computation of the evolution of tensile cracks, of Lazarus (2003)'s variant of this method, and of the present extension to shear mode cracks.

Each simulation consists of two successive steps:

(1) Determination of the SIFs and kernels for the initial crack front considered. This is done using the incremental procedure just sketched, starting from a "reference" penny-shaped crack, for which they are known (see Section 3.3 below), and using a systematic automatic procedure to generate a sequence of successive crack front shapes ending up with that desired.
(2) Determination of the subsequent propagation path. The procedure is basically the same. However successive crack front shapes are no longer arbitrary but deduced sequentially from one another by using the propagation law (22) in the following time-discretized form:

$$\delta a(s,t_i) = \delta a_{\max}\left(\frac{\mathscr{G}(s,t_i)}{\mathscr{G}_{\max}(t_i)}\right)^{\beta/2} \tag{24}$$

The quantity $\delta a_{\max}$ here denotes the maximum crack advance imposed between consecutive steps, and $\mathscr{G}_{\max}(t_i)$ the maximum instantaneous value of the energy release rate along the crack front.[5] (Incidentally, Eq. (24) makes it clear why Paris' propagation law "simulates" that of Griffith in the case of very large exponent β; indeed in such a case $\delta a(s,t_i)$ is nonzero only if $\mathscr{G}(s,t_i)$ is equal to $\mathscr{G}_{\max}(t_i)$).

[5] Some information is lost in Eq. (24) with respect to Eq. (22), namely the instants corresponding to the successive configurations of the crack front. It is of course possible to calculate these instants, as was done by Lazarus (2003) in the case of tensile loadings, but we shall concentrate here on the sole sequence of successive crack front configurations and forget about the corresponding instants.

Details of the numerical procedure for shear loadings are quite similar to those of the procedure for tensile loadings, as expounded by Lazarus (2003), and will not be repeated here. The only significant difference is that the procedure for shear loadings is notably heavier, due to the inevitable coupling of modes 2 and 3. Advantage is however taken of the symmetry property (5), which relates $W_{23}(s,s')$ to $W_{32}(s',s)$ and thus allows to compute and store only W_{23}.

3.3. Initialization: stress intensity factors and fundamental kernels for a penny-shaped crack

The SIFs and kernels for a penny-shaped crack are needed as initial conditions for the numerical procedure just explained. Fig. 3 shows a top view of such a crack, of radius a. (An elliptic crack is also represented for future purposes.) We consider a global right-handed frame $Oxyz$ with origin O at the centre of the crack and axis Oz perpendicular to its plane, together with the associated polar angle θ in the Oxy plane. The curvilinear abscissa $s \equiv a\theta$ along the crack front is oriented in the same way as the polar angle θ. Fig. 3 also shows the local left-handed basis of vectors $(\vec{e}_1, \vec{e}_2(s), \vec{e}_3(s))$ (on the elliptic crack front for legibility), as defined in Section 2.1.1. Note that with the convention adopted, the normal vectors $\vec{e}_1, \vec{e}_z$ to the crack plane are not equal but opposite, so that $[\![\vec{u}]\!](x,y) \equiv \vec{u}(x,y,z=0^-) - \vec{u}(x,y,z=0^+)$. The loading consists of some uniform shear stress $\sigma_{xz} \equiv \tau$ imposed at infinity.

The SIFs and CFWFs for this geometry and loading were given by Tada et al. (1973) and Bueckner (1987), respectively. With the sign conventions adopted, they read as follows:

$$\begin{cases} K_2(\theta) &= -\dfrac{4}{2-\nu}\tau\sqrt{\dfrac{a}{\pi}}\cos\theta \\ K_3(\theta) &= \dfrac{4(1-\nu)}{2-\nu}\tau\sqrt{\dfrac{a}{\pi}}\sin\theta \end{cases} \tag{25}$$

$$\begin{cases} W_{22}(\theta_1,\theta_2) = \dfrac{2\cos(\theta_1-\theta_2)-3\nu}{2-\nu} \\ W_{33}(\theta_1,\theta_2) = \dfrac{2(1-\nu)\cos(\theta_1-\theta_2)+3\nu}{2-\nu} \\ W_{23}(\theta_1,\theta_2) = \dfrac{1}{1-\nu}W_{32}(\theta_2,\theta_1) = \dfrac{2\sin(\theta_1-\theta_2)}{2-\nu} \end{cases} \tag{26}$$

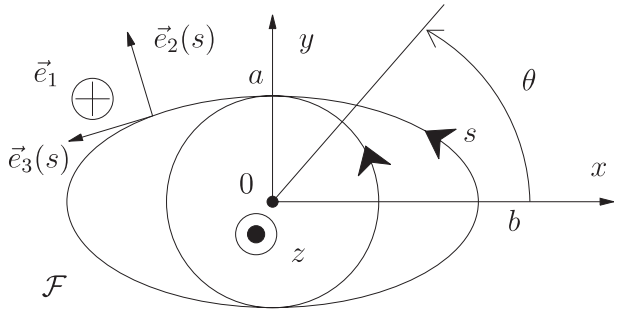

Fig. 3. Top views of penny-shaped and elliptic cracks.

4. Validation: calculation of shear mode stress intensity factors for an elliptic crack

In order to assess the accuracy of the numerical procedure proposed, we shall apply it to the calculation of the SIFs along the front of some elliptic crack obtained through gradual deformation of an initially penny-shaped crack, and compare the results with the known analytic solution. This solution was provided by Kassir and Sih (1966). For an elliptic crack of minor axis a, parallel to the Oy axis, and major axis b, parallel to the Ox axis (see Fig. 3), loaded through some uniform remote shear stress $\sigma_{xz} \equiv \tau$, it reads as follows:

$$\begin{cases} K_2(\theta) = -\dfrac{\alpha^2 f(k,\nu)\cos\theta}{(\sin^2\theta + \alpha^4\cos^2\theta)^{1/4}(\sin^2\theta + \alpha^2\cos^2\theta)^{1/4}}\tau\sqrt{\pi a} \\ K_3(\theta) = \dfrac{(1-\nu) f(k,\nu)\sin\theta}{(\sin^2\theta + \alpha^4\cos^2\theta)^{1/4}(\sin^2\theta + \alpha^2\cos^2\theta)^{1/4}}\tau\sqrt{\pi a} \end{cases} \tag{27}$$

In these expressions θ denotes the polar angle as above (*not* the angle of the classical parametric equations of the ellipse, $x = b\cos\phi$, $y = a\sin\phi$); also, α, k and $f(k,\nu)$ are defined by

$$\alpha \equiv \frac{a}{b}; \quad k \equiv \sqrt{1-\alpha^2}; \quad f(k,\nu) \equiv \frac{k^2}{(k^2-\nu)E(k) + \nu(1-k^2)K(k)} \tag{28}$$

where $K(k)$ and $E(k)$ are the complete elliptic integrals of the first and second kinds (Gradsteyn and Ryzhik, 1965).

Fig. 4 shows theoretical and numerical results for elliptic cracks of various shapes, for a Poisson's ratio of 0.25. The origin of the curvilinear abscissa here is taken at the right endpoint of the major axis. In the numerical calculations, each ellipse is discretized with 200 points, and the maximum stepsize for each increment of deformation of the crack front is $\delta a_{\max} = 2.5 \times 10^{-3} a$.

Table 1 also displays the mean errors E_2, E_3 defined as

$$E_i \equiv \left\{ \frac{1}{L}\int_0^L \frac{(K_i^{\text{num}}(s) - K_i^{\text{theor}}(s))^2}{4\tau^2 a/\pi}\,\mathrm{d}s \right\}^{1/2} \quad (i = 2, 3) \tag{29}$$

where L is the perimeter of the ellipse.

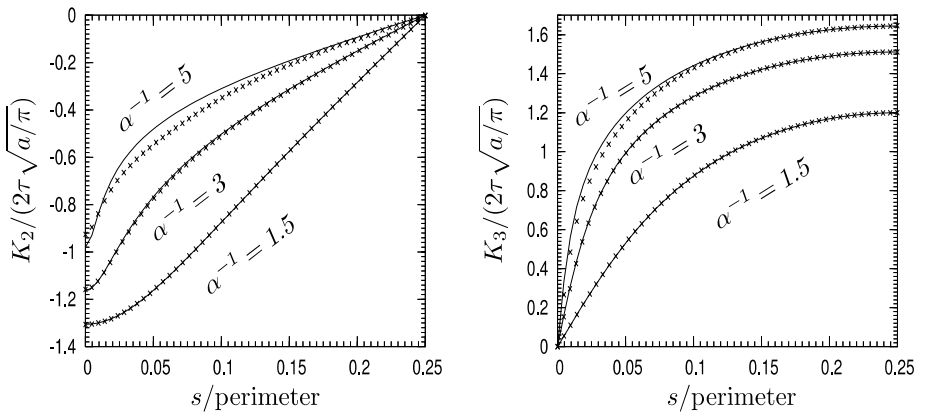

(a) Mode 2 SIF **(b)** Mode 3 SIF

Fig. 4. Shear mode SIFs along the front of various elliptic cracks—Lines: analytical formulae (27); discrete points: numerical results.

Table 1
Mean errors made in the numerical calculation of shear mode SIFs for elliptic cracks

	$\alpha^{-1}=1.5$	$\alpha^{-1}=3$	$\alpha^{-1}=5$
E_2	5.7×10^{-4}	8.7×10^{-3}	4.6×10^{-2}
E_3	3.3×10^{-4}	4.3×10^{-3}	3.2×10^{-2}

Fig. 4 and Table 1 exhibit a good agreement between numerical and theoretical results, even though the errors of course increase with the eccentricity of the ellipse. Also, these errors are larger than those found by Lazarus (2003) when performing similar calculations in mode 1. This can rationalized by the fact that more calculations, introducing more inaccuracies, are required in mode $2+3$: indeed for mode 1 two integrals must be evaluated at each step (one for δK_1 plus one for δW_{11}), versus ten for mode $2+3$ (two for each δK_i, $i=2,3$, plus two for each δW_{ij}, $(i,j)=(2,2),(3,3),(2,3)$).

The errors in Fig. 4 and Table 1 are comparable to those made using the FEM for ellipses with large eccentricities, and notably smaller for ellipses with moderate eccentricities. For instance Sukumar et al. (2003), using the level set method coupled with the XFEM, reported a relative error of 2×10^{-2} in the calculation of K_1 for an elliptic crack with $\alpha^{-1}=2$. This is notably larger than the error reported in Table 1 for mode $2+3$, which is itself larger than that reported by Lazarus (2003) for mode 1.

5. Application to simulation of propagation of shear mode cracks

5.1. Propagation of initially circular, elliptic, rectangular and heart-shaped cracks in fatigue and brittle fracture

We have computed the successive shapes of initially circular, elliptic, rectangular and heart-shaped cracks obeying the propagation law (22). The value of Poisson's ratio used was $\nu=0.25$, and that of Paris' exponent was $\beta=2$ for fatigue and $\beta=50$ ($\approx+\infty$) for brittle fracture. The simulations were stopped when the crack reached a stable shape. Figs. 5 and 6 show the successive crack configurations obtained. The quantity a here denotes a typical dimension of the initial crack shape, the precise definition of which depends on this shape and is conspicuous on the figures.

The difference between successive crack fronts in fatigue and brittle fracture clearly appears in these figures. In fatigue, all points of the crack front move simultaneously. In brittle fracture, propagation occurs only on some "active" part of the front. This active part starts from those points where the energy release rate is initially maximum, and gradually extends over the crack front. The stable crack shape is reached as soon as the whole front has become active.

The stable shape can be observed to be approximately elliptic in all cases; this question will be examined in more detail in the next section. However, in the cases of initially rectangular and heart-shaped cracks, which are numerically tricky because of the presence of angular points on the crack front, one can observe some slight perturbation of the regular shape of the front in the vicinity of these points. This perturbation is due to numerical errors, and therefore provides an appreciation of the accuracy of the method. It clearly appears here that numerical errors accumulate and cannot be corrected for once they are made. This unhappy feature of the numerical procedure of course arises from its incremental nature, and is in clear contrast with those of more classical procedures such as the FEM. It is a counterpart of the simplicity and efficiency of the method.

It is also interesting to note that in the case of propagation of an initially heart-shaped crack in brittle fracture (last diagram of Fig. 6), even when the crack front has reached its stable shape, it does not move symmetrically with respect to its vertical axis of symmetry; the propagation rate is larger on its right part than on its left one. The explanation of this apparent paradox is that in brittle fracture, the motion of the

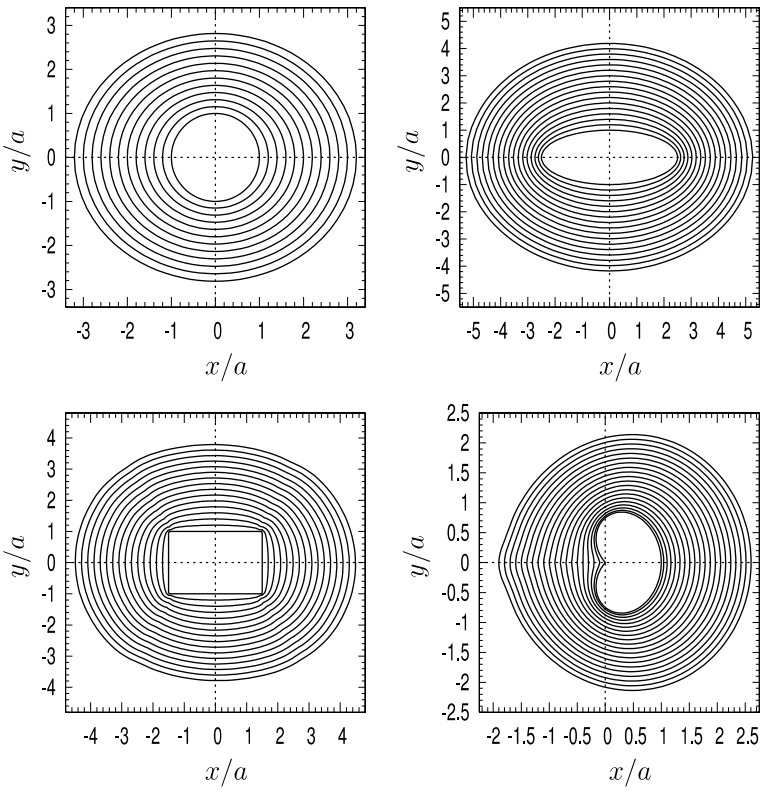

Fig. 5. Successive crack fronts of shear mode cracks in fatigue ($\beta = 2$).

crack front is not defined in a unique way, because the distribution of the energy release rate along the crack front is insensitive to global translational motions of this front; the simulation thus "selects" some possible solution among the very many envisageable, in which the left and right parts of the crack front happen to propagate at different rates. The selection of this specific solution is governed by the initial crack front shape, which is itself not symmetric. A subtle difference appears here between Griffith's original propagation law and its "regularized" variant used here, that is Paris' law with a very large exponent: Griffith's law implies some bifurcation, but this bifurcation is erased by the regularization, just as bifurcations occurring in plasticity are erased by viscoplastic regularizations of the flow rule.

5.2. Theoretical study of the stable shape of the crack front

The aim of this section is to show that the stable shape of the crack front is only *approximately* elliptic, and also to derive an approximate, but accurate analytical formula for the ratio of the axes of this stable shape based on the approximation that it *is* elliptic.

Let $\theta \mapsto r_0(\theta)$ denote the polar representation of the stable shape. Since this shape is preserved in time, the polar representation of the crack front is of the form $\theta \mapsto r(\theta, t) \equiv \lambda(t) r_0(\theta)$ at each instant. For such a propagation path, the normal velocity of the crack front is given by

$$\frac{\partial a}{\partial t}(\theta, t) \equiv \frac{\partial r}{\partial t}(\theta, t)\vec{e}_r(\theta, t) \cdot \vec{e}_2(\theta, t) = \lambda'(t) \frac{r_0^2(\theta)}{\sqrt{r_0'^2(\theta) + r_0^2(\theta)}} \tag{30}$$

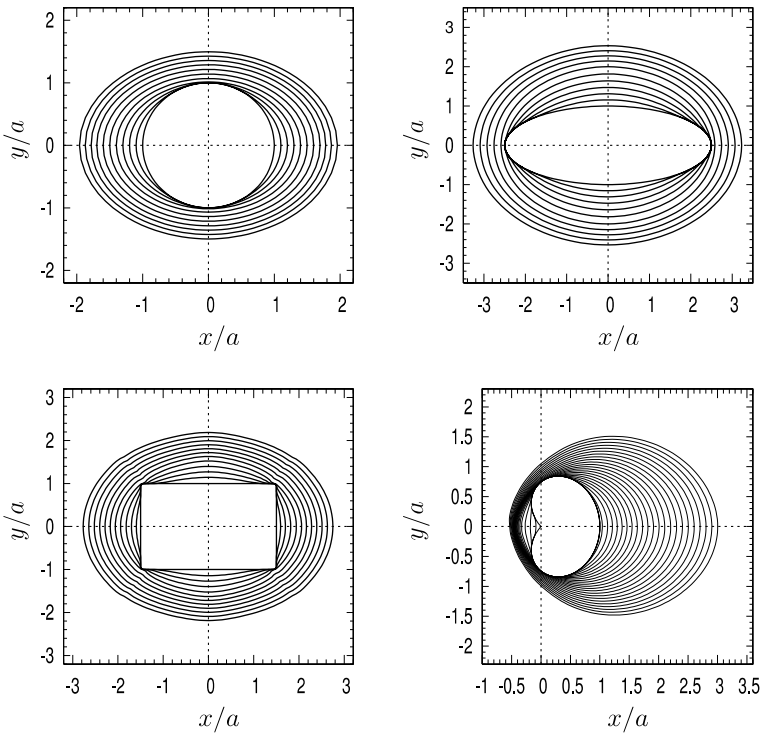

Fig. 6. Successive crack fronts of shear mode cracks in brittle fracture ($\beta = 50$).

Paris' propagation law (22) then implies that

$$\mathscr{G}(\theta,t) \propto \left(\frac{r_0^2(\theta)}{\sqrt{r_0'^2(\theta) + r_0^2(\theta)}} \right)^{2/\beta} \tag{31}$$

Now, for an elliptic crack,

$$r(\theta) = \frac{a}{\sqrt{\sin^2\theta + \alpha^2\cos^2\theta}} \tag{32}$$

and, by Eqs. (23) and (27)

$$\frac{E\mathscr{G}(\theta)}{(1-\nu^2)\tau^2\pi a} = [f(k,\nu)]^2 \frac{\alpha^4\cos^2\theta + (1-\nu)\sin^2\theta}{(\sin^2\theta + \alpha^4\cos^2\theta)^{1/2}(\sin^2\theta + \alpha^2\cos^2\theta)^{1/2}} \tag{33}$$

Eq. (31), with $r_0(\theta)$ given by an expression of type (32), and Eq. (33) stipulate different types of dependence of $\mathscr{G}$ upon θ, whatever the value of Paris' exponent β. Hence the stable shape cannot be elliptic.

However, it has already been noted upon inspection of Figs. 5 and 6 that the elliptic shape is a good approximation to the true stable shape. Accepting this approximation, one can derive an again approximate but accurate formula for the ratio of the axes of the stable shape. Indeed, since this ratio does not vary in time,

$$\frac{(\partial a/\partial t)(\theta = \pi/2, t)}{(\partial a/\partial t)(\theta = 0, t)} = \frac{a}{b} \tag{34}$$

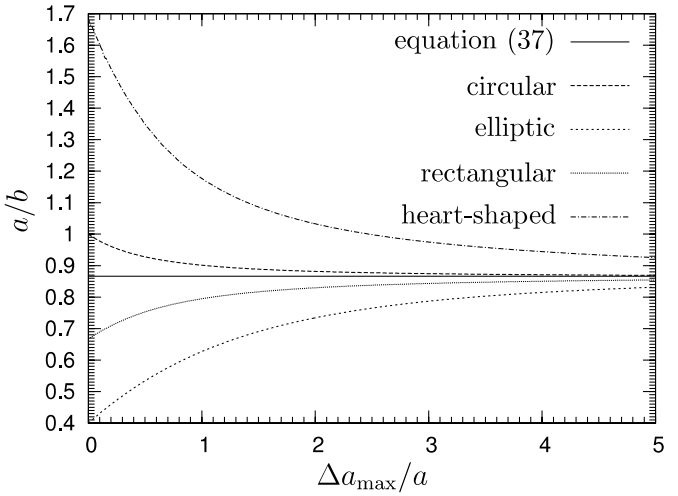

Fig. 7. Evolution of the ratio of the axes of the crack in fatigue ($\beta = 2$).

Also, Paris' propagation law (22) implies that

$$\frac{(\partial a/\partial t)(\theta = \pi/2, t)}{(\partial a/\partial t)(\theta = 0, t)} = \left(\frac{\mathcal{G}(\theta = \pi/2, t)}{\mathcal{G}(\theta = 0, t)}\right)^{\beta/2} \tag{35}$$

Now if the crack is nearly elliptic,

$$\frac{\mathcal{G}(\theta = \pi/2)}{\mathcal{G}(\theta = 0)} \approx (1 - \nu)\frac{b}{a} \tag{36}$$

by Eq. (33). Combining Eqs. (34)–(36), one gets

$$\frac{a}{b} \approx (1 - \nu)^{\frac{\beta}{\beta+2}} \tag{37}$$

The special case where $\beta = +\infty$ (brittle fracture) was considered by Gao (1988), using a first-order perturbation approach based on the assumption of a nearly circular stable shape. He found that for this stable shape,

$$\frac{a}{b} \approx 1 - 2A, \quad A \equiv \frac{\nu(2 - \nu)}{2(2 - 2\nu - \nu^2)} \tag{38}$$

The deviation from a circular shape in this formula is proportional to A and therefore to ν. Thus the perturbation approach is valid only provided that Poisson's ratio is much smaller than unity, and only zeroth- and first-order terms in ν must in fact be retained in formula (38).[6] This formula then reduces to

$$\frac{a}{b} \approx 1 - \nu \tag{39}$$

and this agrees with Eq. (37) for $\beta = +\infty$.

Figs. 7 and 8 show the evolution of the ratio a/b as a function of $\Delta a_{\max}/a$, $\Delta a_{\max}$ denoting the maximum crack advance, for the various initial crack shapes envisaged, in both fatigue and brittle fracture. This ratio

[6] This point seems to have been overlooked by Gao (1988).

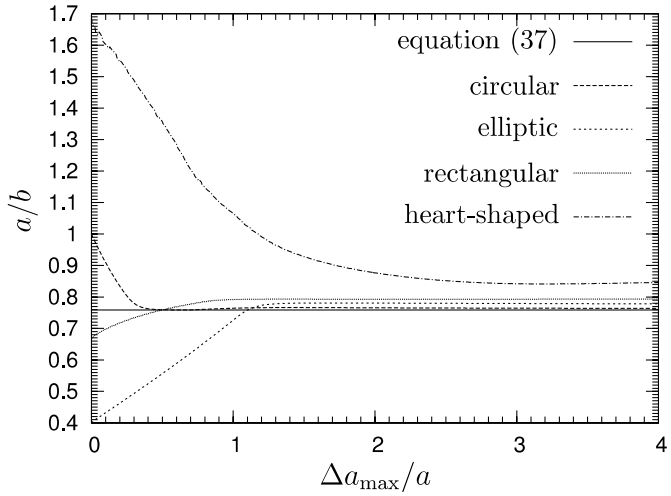

Fig. 8. Evolution of the ratio of the axes of the crack in brittle fracture ($\beta = 50$).

Table 2
Values of $\frac{|(a/b)_{num} - (a/b)_{lim}|}{(a/b)_{lim}}$ in fatigue and brittle fracture

	$\beta = 2$ (%)	$\beta = 50$ (%)
Circular	0.3	0.7
Elliptic	4	2.8
Rectangular	1.3	4.8
Heart-shaped	6.8	11.6

can be observed to tend toward some limit independent of the initial crack shape and in acceptable agreement with the theoretical value provided by Eq. (37).

Table 2 allows to better appreciate the convergence of numerical values of a/b toward their theoretical limit given by Eq. (37). It shows the relative gap between this theoretical limit value and that obtained numerically after an maximum advance of $5a$ in the case of fatigue, and $4a$ in the case of brittle fracture. It can be observed that convergence is slowest for the initially heart-shaped crack in both fatigue and brittle fracture. The obvious explanation is that this is the initial crack shape that differs most markedly from the stable, quasi-elliptic crack shape. Also, the agreement between numerical and theoretical limit values of a/b is better for $\beta = 2$ than for $\beta = 50$. This is again no surprise because for very large values of β, the local propagation rate is very sensitive to the local value of the energy release rate, and this enhances the impact of numerical errors.

6. Summary and conclusion

This paper was devoted to numerical simulation of coplanar propagation (channeled along some weak planar layer) of shear mode cracks with arbitrary contour. The crack was assumed to be embedded in some infinite body loaded through uniform remote stresses. Propagation laws pertaining to both brittle fracture and fatigue were envisaged.

We first derived formulae providing, to first order, the variations of the three stress intensity factors resulting from a small but otherwise arbitrary coplanar perturbation of the crack front, under conditions of constant prescribed loading. The expressions of these variations consisted of integrals along the crack front involving some matrix "kernel" linked to the crack face weight functions, plus some "local" terms. The first-order expressions of the variations of the components of this kernel were also derived.

These results were then used to extend Lazarus (2003)'s simplified variant of Bower and Ortiz (1990, 1991, 1993)'s method for numerical simulation of coplanar propagation of mode 1 cracks to mixed-mode (2 + 3) cracks. The propagation paths of initially circular, elliptic, rectangular and heart-shaped shear mode cracks were studied in both fatigue and brittle fracture. These simulations evidenced the existence of some almost elliptic stable crack front shape, toward which all the crack fronts considered were observed to evolve. An approximate but accurate formula providing the ratio of the axes of this stable shape as a function of Poisson's ratio and Paris' exponent was finally derived.

Appendix A. Justification of formula (11)

The aim of this appendix is to calculate the limit in the left-hand side of Eq. (11) of the text.

It is recalled that the crack advance δa in this formula is assumed to be zero at the point s_0. Without any loss of generality, we can assume that $s_0 = 0$. Also, we split the integration domain $(-\infty, +\infty)$ into $[(-\infty, -\eta) \cup (\eta, +\infty)] \cup [-\eta, \eta]$, η being an arbitrary positive number. This number is fixed for the moment but will go to zero at the end of the reasoning.

Consider the integral over $(-\infty, -\eta) \cup (\eta, +\infty)$ first. For any fixed s in this domain, the quantity $k_{ji}(\mathscr{F}; s; s_0, r)/\sqrt{r} \equiv k_{ji}(\mathscr{F}; s; 0, r)/\sqrt{r}$ has a finite limit for $r \to 0$ given by Eq. (3). Hence

$$\lim_{r\to 0} \frac{1}{\sqrt{r}} \int_{(-\infty,-\eta)\cup(\eta,+\infty)} k_{ji}(\mathscr{F}; s; 0, r) K_m(s) \delta a(s)\, \mathrm{d}s = \frac{1}{\pi}\sqrt{\frac{2}{\pi}} \int_{(-\infty,-\eta)\cup(\eta,+\infty)} \frac{W_{ji}(s,0)}{D^2(s,0)} K_m(s) \delta a(s)\, \mathrm{d}s \tag{A.1}$$

Note that the term $D^2(s,0)$ in the denominator here does not raise any problem of convergence of the integral since it never becomes zero in the domain $(-\infty, -\eta) \cup (\eta, +\infty)$.

Taking the limit of the integral over $[-\eta, \eta]$ is more difficult because $D^2(s,0)$ vanishes on this interval at the point $s_0 = 0$. Performing a first-order Taylor expansion of the quantity $K_m(s)\delta a(s)$ around this point in this integral, one gets

$$\begin{aligned} &\frac{1}{\sqrt{r}} \int_{-\eta}^{\eta} k_{ji}(\mathscr{F}; s; 0, r) K_m(s) \delta a(s)\, \mathrm{d}s \\ &\quad = K_m(0)\delta a'(0) \int_{-\eta}^{\eta} \frac{k_{ji}(\mathscr{F}; s; 0, r)}{\sqrt{r}} s\, \mathrm{d}s + \int_{-\eta}^{\eta} \frac{k_{ji}(\mathscr{F}; s; 0, r)}{\sqrt{r}} \mathrm{O}(s^2)\, \mathrm{d}s \end{aligned} \tag{A.2}$$

Now in the special cases where the CFWFs are known explicitly, that is for a semi-infinite crack (Gao and Rice, 1986), a penny-shaped crack (Gao, 1988) and an external circular crack loaded in mode 1 (Gao and Rice, 1987), the quantities $k_{ji}(\mathscr{F}; s; 0, r)/\sqrt{r}$ are bounded by a constant times s^{-2} for $s \to 0$. Making the reasonable assumption that this is true in general, we conclude that the integrand in the second term of the right-hand side of Eq. (A.2) is O(1) for $s \to 0$, so that this equation may be rewritten as

$$\frac{1}{\sqrt{r}} \int_{-\eta}^{\eta} k_{ji}(\mathscr{F}; s; 0, r) K_m(s) \delta a(s)\, \mathrm{d}s = K_m(0)\delta a'(0) \int_{-\eta}^{\eta} \frac{k_{ji}(\mathscr{F}; s; 0, r)}{\sqrt{r}} s\, \mathrm{d}s + \mathrm{O}(\eta) \tag{A.3}$$

In order to calculate the limit of the integral in the right-hand side of Eq. (A.3), let us use the property of positive homogeneity of degree $-3/2$ of the CFWFs and the change of variable $s' \equiv s/r$; we thus get

$$\int_{-\eta}^{\eta} \frac{k_{ji}(\mathscr{F};s;0,r)}{\sqrt{r}} s\,\mathrm{d}s = \int_{-\eta/r}^{\eta/r} k_{ji}(\mathscr{F}/r;s';0,1)s'\,\mathrm{d}s' \tag{A.4}$$

The $k_{ji}(\mathscr{F}/r;s';0,1)$ here represent the CFWFs at the observation point s', when unit point forces are exerted on the crack faces at a distance of unity from the point $s_0 = 0$ of the crack front $\mathscr{F}$, this front being "dilated" by a factor of $1/r$. In the limit $r \to 0$, the curvature of this dilated front becomes zero, so that the $k_{ji}(\mathscr{F}/r;s';0,1)$ become identical to the CFWFs of a half-plane crack. Also, the lower and upper bounds $\pm\eta/r$ of the integral go to $\pm\infty$. Using the well-known expressions of the CFWFs for a half-plane crack (Gao and Rice, 1986), one then gets

$$\lim_{r\to 0} \int_{-\eta}^{\eta} \frac{k_{ji}(\mathscr{F};s;0,r)}{\sqrt{r}} s\,\mathrm{d}s = \begin{cases} 0 & \text{if } (j,i) = (2,2) \text{ or } (3,3) \\ \sqrt{\dfrac{1}{2\pi}}\dfrac{4\nu}{2-\nu} & \text{if } (j,i) = (2,3) \text{ or } (3,2) \end{cases} \tag{A.5}$$

Combination of Eqs. (A.3) and (A.5) then yields

$$\lim_{r\to 0} \frac{1}{\sqrt{r}} \int_{-\eta}^{\eta} k_{ji}(\mathscr{F};s;0,r) K_m(s)\delta a(s)\,\mathrm{d}s = \sqrt{\frac{1}{2\pi}}\frac{4\nu}{2-\nu}(\delta_{j2}\delta_{i3} + \delta_{j3}\delta_{i2})K_m(0)\delta a'(0) + \mathrm{O}(\eta) \tag{A.6}$$

Combining Eqs. (A.1) and (A.6), and then letting η go to zero, one finally gets Eq. (11) of the text (with $s_0 = 0$).

References

Bonnet, M., 1994. Equations intégrates et éléments de frontière en mécanique des solides. Ecole Polytechnique (Palaiseau), Ch. 2 et 5.

Bower, A.F., Ortiz, M., 1990. Solution of three-dimensional crack problems by a finite perturbation method. Journal of the Mechanics and Physics of Solids 38 (4), 443–480.

Bower, A.F., Ortiz, M., 1991. A three-dimensional analysis of crack trapping and bridging by tough particles. Journal of the Mechanics and Physics of Solids 39 (6), 815–858.

Bower, A.F., Ortiz, M., 1993. An analysis of crack trapping by residual stresses in brittle solids. Transactions of the ASME. Journal of Applied Mechanics 60 (1), 175–182.

Bueckner, H.F., 1970. A novel principle for the computation of stress intensity factors. Zeitschrift fur Angewandte Mathematik und Mechanik 50 (9), 529–546.

Bueckner, H.F., 1973. Field singularities and related integral representations (crack analysis). In: Sih, G.C. (Ed.), Mechanics of Fracture, vol. 1, Methods of Analysis and Solutions of Crack Problems. Noordhoff, Leyden, The Netherlands.

Bueckner, H.F., 1987. Weight functions and fundamental fields for the penny-shaped and the half-plane crack in three-space. International Journal of Solids and Structures 23 (1), 57–93.

Fares, N., 1989. Crack fronts trapped by arrays of obstacles: numerical solutions based on surface integral representation. Transactions of the ASME. Journal of Applied Mechanics 56 (4), 837–843.

Gao, H., 1988. Nearly circular shear mode cracks. International Journal of Solids and Structures 24 (2), 177–193.

Gao, H., Rice, J.R., 1986. Shear stress intensity factors for planar crack with slightly curved front. ASME Journal of Applied Mechanics 53 (4), 774–778.

Gao, H., Rice, J.R., 1987. Nearly circular connections of elastic half spaces. ASME Journal of Applied Mechanics 54 (4), 627–634.

Gradsteyn, I.S., Ryzhik, I.M., 1965. Tables of Integrals Series, and Products. Academic Press, New York.

Gravouil, A., Moes, N., Belytschko, T., 2002. Non-planar 3d crack growth by the extended finite element and level sets. II. Level set update. International Journal for Numerical Methods in Engineering 53 (11), 2569–2586.

Kassir, M.K., Sih, G.C., 1966. Three-dimensional stress distribution around an elliptical crack under arbitrary loadings. ASME Journal of Applied Mechanics 33 (3), 601–611.

Lazarus, V., 2003. Brittle fracture and fatigue propagation paths of 3D plane cracks under uniform remote tensile loading. International Journal of Fracture 112 (1–2), 23–46.

Leblond, J.-B., Lazarus, V., Mouchrif, S.-E., 1999. Crack paths in three-dimensional elastic solids. II. Three-term expansion of the stress intensity factors—Applications and perspectives. International Journal of Solids and Structures 36 (1), 105–142.

Moes, N., Gravouil, A., Belytschko, T., 2002. Non-planar 3d crack growth by the extended finite element and level sets. I. Mechanical model. International Journal for Numerical Methods in Engineering 53 (11), 2549–2568.

Rice, J.R., 1972. Some remarks on elastic crack-tip stress fields. International Journal of Solids and Structures 8 (6), 751–758.

Rice, J.R., 1985. First-order variation in elastic fields due to variation in location of a planar crack front. ASME Journal of Applied Mechanics 52 (3), 571–579.

Rice, J.R., 1989. Weight function theory for three-dimensional elastic crack analysis. In: Wei, R.P., Gangloff, R.P. (Eds.), Fracture Mechanics: Perspectives and Directions (Twentieth Symposium). American Society for Testing and Materials STP 1020, Philadelphia, USA.

Sukumar, N., Chopp, D.L., Moran, B., 2003. Extended finite element method and fast marching method for three-dimensional fatigure crack propagation. Engineering Fracture Mechanics 70 (1), 29–48.

Tada, H., Paris, P.C., Irwin, G.R., 1973. The Stress Analysis of Cracks Handbook. Del Research Corporation, Hellertown, USA.

Xu, G., Ortiz, M., 1993. A variational boundary integral method for the analysis of 3-d cracks of arbitrary geometry modelled as continuous distributions of dislocation loops. International Journal for Numerical Methods in Engineering 36 (21), 3675–3701.

Xu, G., Bower, A., Ortiz, M., 1994. An analysis of non-planar crack growth under mixed mode loading. International Journal of Solids and Structures 31 (16), 2167–2193.